Resonant inelastic x-ray scattering studies of elementary excitations

Ament, L.J.P.

Chapter 6

RIXS in systems with strong spin-orbit coupling

Published as '*Resonant Inelastic X-ray Scattering on Spin-Orbit Coupled Insulating Iridates*', arXiv:1008.4862, with Giniyat Khaliullin and Jeroen van den Brink

6.1 Introduction

In the introduction of chapter 5, it was noted that one way to lift the ground state orbital degeneracy is by relativistic spin-orbit coupling. Relativistic spin-orbit coupling is strong in the heavier elements such as iridium – the subject of this chapter.

More specifically, we focus on compounds where the Ir ion has a charge of 4+, *i.e.*, it is in a $5d^5$ configuration. The Kramers degeneracy theorem states that the energy levels of a system with an odd number of electrons remain at least doubly degenerate in the absence of magnetic fields [211]. This implies that spin-orbit coupling cannot remove all degeneracy of the Ir^{4+} ion. As a matter of fact, as shown in Sec. 6.2, the ground state is a Kramers doublet: its two degenerate states are each other's time reversed states, and it can be represented by a pseudo-spin-1/2.

Because the two states in the Kramers doublet have exactly the same charge distribution, Jahn-Teller couplings cannot lift their degeneracy. Superexchange coupling, however, is present in the Mott insulating Ir compounds.

The strong spin-orbit interaction can cause entirely new kinds of ordering in the combined orbital-spin sector which are of a topological nature. This was recently proposed for certain iridium-oxides [212,213], members of a large family of iridium-based materials. Na_2IrO_3, for instance, is predicted to be a topological insulator exhibiting the quantum spin Hall effect at room temperature [212]. The topologically non-trivial state arises from the presence of complex hopping integrals, resulting from the unquenched iridium orbital moment. This system can also be described in terms of a Mott insulator, with interactions between the effective iridium spin-orbital degrees of freedom that are given by the Kitaev-Heisenberg model [214, 215]. In the pyrochlore iridates $A_2Ir_2O_7$ (where A is a 3+ ion), a quantum phase transition from a topological band insulator to a topological Mott insulator has been proposed as a function of the electron-electron interaction strength [213].

To establish whether and how such novel phases are realized in iridium oxides it is essential to probe and understand their spin-orbital ordering and related elementary excitations. In this context it is advantageous to consider the structurally less complicated, single-layer iridium perovskite Sr_2IrO_4. This material is in many respects the analog of the high-T_c cuprate parent compound La_2CuO_4 [214]. Structurally it is identical, with the obvious difference that the Ir $5d$ valence electrons are, as opposed to the Cu $3d$ electrons, very strongly spin-orbit coupled. The similarity cuts deeper, however, as the low energy sector of the iridates is spanned by local spin-orbit doublets with an effective spin of $1/2$, which reside on a square lattice and interact via superexchange – a close analogy with the undoped cuprates. This observation motivates doping studies of Sr_2IrO_4 searching for superconductivity [216,217]. Experimentally, however, far less is known about the microscopic ordering and excitations in iridates than in cuprates. Inelastic neutron scattering, which can in principle reveal such properties, is not possible because Ir is a strong neutron absorber and, moreover, crystals presently available tend to be tiny. As a consequence not even the interaction strength between the effective spins in the simplest iridium-oxides is established: estimates for Sr_2IrO_4, for instance, range from $\sim$50 meV [214] to $\sim$110 meV [218].

In this chapter we show that while for iridates neutron scattering falls short, RIXS fills the void: RIXS at the iridium L edge offers direct access to the excitation spectrum across the Brillouin zone, enabling one to measure the dispersion of elementary magnetic excitations. Besides the low energy magnons related to long-range order of the doublets, RIXS will also reveal the dynamics of higher energy, doublet to quartet, spin-orbit excitations. This allows to directly test theoretical models for the excitation spectra and extract accurate values of the superexchange and spin-orbit coupling constants J and λ, respectively. This chapter deals with the RIXS spectrum of insulating iridates in general, and of Sr_2IrO_4 in particular. Sec. 6.2 reviews the different models for Sr_2IrO_4 (the strong spin-orbit coupling model outlined above and the crystal field model for Ir ions in a D_{4h} crystal field). Sec. 6.3 describes the dipole operators that appear in RIXS

at the Ir^{4+} L edge. In the remainder of that section, the local effective scattering operators are derived, neglecting intermediate state dynamics. The results of this section apply to all Ir^{4+} compounds with octahedral crystal fields (provided spin-orbit coupling also dominates). Then, Sec. 6.3.3 calculates the RIXS spectrum of Sr_2IrO_4 within the strong spin-orbit coupling limit. The Kramers doublet gives single- and two-pseudo-magnon excitations, while excitations from the Kramers doublet to the higher energy quartet are assumed to be local excitations.

6.2 Theory of Sr_2IrO_4

As noted in Sec. 2.2.2, the relativistic spin-orbit coupling in atoms is proportional to Z^4, where Z is the atomic number: in the heavier elements, spin-orbit coupling becomes more and more important. In iridium, the element that is studied in this chapter, the spin-orbit coupling λ is estimated to be as large as 380 meV in Ir^{4+} ions [219]. When the crystal field and superexchange interactions are small, the relativistic spin-orbit coupling can dominate the physics of materials containing Ir. Examples of such materials are Sr_2IrO_4, which will be studied in this chapter, Na_2IrO_3 [212, 214], and pyrochlore iridates $A_2Ir_2O_7$ (where A is a 3+ ion) [213].

Sr_2IrO_4 is a Mott insulator, although not a very good one: the optical gap is only ~ 0.4 eV [220]. It is a layered perovskite compound: each layer consists of a square lattice of Ir ions in a $5d^5$ configuration. The Ir ions are located in octahedra of oxygen ions, who split the d levels by ~ 3 eV into e_g and t_{2g} states [221]. This 10Dq splitting is strong enough to enforce that the lowest energy configuration is t_{2g}^5 [222, 223]. Thus, Sr_2IrO_4 can be regarded as the t_{2g} analog of La_2CuO_4 [214]. The local ground state of the hole in the t_{2g} shell could be dictated by the remaining crystal field (the octahedra are elongated along the z direction, favoring $|xy\rangle$), by superexchange interactions (as in the titanates described in chapter 5), or by the relativistic spin-orbit coupling.

The spin-orbit coupling $\lambda \approx 380$ meV [219] is much larger than intersite exchange interactions could generate. Jackeli and Khaliullin [214] derive a superexchange constant of 45 meV from the magnetic ordering temperature: an order of magnitude smaller than λ. Further, resonant X-ray scattering (RXS) data contradicts the crystal field scenario, and is in agreement with dominant spin-orbit coupling [223].

We first investigate the case that spin-orbit coupling dominates the low energy physics of the t_{2g}^5 configuration. The 10Dq splitting is larger by an order of magnitude than λ, and therefore we assume that the t_{2g} hole does not hybridize with the e_g orbitals through the spin-orbit coupling. The orbital degree of freedom of the hole is then described by an effective angular momentum $l = 1$ [25]. The true orbital angular momentum $\mathbf{L} = -\mathbf{l}$, and when the spin-orbit coupling term is projected to the t_{2g} subspace, it becomes $-\lambda \mathbf{l} \cdot \mathbf{S}$ with $\lambda > 0$. Note that electron states are considered here, instead of hole state

as in Ref. [214]. The eigenstates of the spin-orbit coupling single ion Hamiltonian $H_0 = -\lambda \mathbf{l}\cdot\mathbf{S}$ are characterized by the total effective angular momentum $\mathbf{J}_{\rm eff} = \mathbf{S} + \mathbf{l}$: $H_0 = -\lambda\left[\mathbf{J}_{\rm eff}^2 - \mathbf{l}^2 - \mathbf{S}^2\right]/2 = -\lambda\left[J_{\rm eff}(J_{\rm eff}+1)/2 - 11/8\right]$. The eigenstates form a doublet with $J_{\rm eff} = 1/2$ at energy λ and a quartet with $J_{\rm eff} = 3/2$ at energy $-\lambda/2$. In the t_{2g}^5 ground state, the quartet is completely filled while the doublet contains a single electron.

Next, we incorporate lattice distortions in the model. They add a term $-\Delta l_z^2$ to H_0, with $\Delta > 0$ for elongation of the octahedra along the z axis. This lowers the zx and yz states in energy, relative to the xy orbital. The $J_{\rm eff} = 1/2$ Kramers doublet remains unsplit and becomes [214]

$$\left|\tilde{\uparrow}\right\rangle = \sin\theta\,|0\uparrow\rangle - \cos\theta\,|{+1}\downarrow\rangle \qquad \text{and} \qquad \left|\tilde{\downarrow}\right\rangle = \sin\theta\,|0\downarrow\rangle - \cos\theta\,|{-1}\uparrow\rangle \quad (6.1)$$

with $\tan 2\theta = 2\sqrt{2}\lambda/(\lambda - 2\Delta)$, and where the orbital states are indexed by $l_z = -1, 0, +1$. The corresponding orbital annihilation operators $d_{-1,0,1}$ are defined by the relations

$$\begin{aligned} d_{yz} &= -\tfrac{1}{\sqrt{2}}(d_1 - d_{-1}), \\ d_{zx} &= \tfrac{i}{\sqrt{2}}(d_1 + d_{-1}), \\ d_{xy} &= d_0. \end{aligned} \quad (6.2)$$

The energy of the doublet is $E_f = \lambda/(\sqrt{2}\tan\theta)$. The $J_{\rm eff} = 3/2$ quartet splits into two doublets: $\{|1\uparrow\rangle\,,\ |{-1}\downarrow\rangle\}$ at energy $E_g = -\Delta - \lambda/2$ and $\{\cos\theta\,|0\uparrow\rangle + \sin\theta\,|1\downarrow\rangle\,,\ \cos\theta\,|0\downarrow\rangle + \sin\theta\,|{-1}\uparrow\rangle\}$ at energy $E_h = -(\lambda\tan\theta)/\sqrt{2}$.

The three doublets are conveniently denoted by the three fermions f, g, h, where the pseudo-spin labels the two states within the doublets. We introduce their annihilation operators

$$\begin{array}{lll} f_\uparrow = \sin\theta\ d_{0\uparrow} - \cos\theta\ d_{1\downarrow}, & g_\uparrow = d_{1\uparrow}, & h_\uparrow = \cos\theta\ d_{0\uparrow} + \sin\theta\ d_{1\downarrow}, \\ f_\downarrow = \sin\theta\ d_{0\downarrow} - \cos\theta\ d_{-1\uparrow}, & g_\downarrow = d_{-1\downarrow}, & h_\downarrow = \cos\theta\ d_{0\downarrow} + \sin\theta\ d_{-1\uparrow}. \end{array} \quad (6.3)$$

Their energies were already denoted as $E_{f,g,h}$ above.

Now, we take two limits: the one suggested by Ref. [214] and supported by the RXS experiment of Ref. [223] which supposes that spin-orbit coupling dominates ($\Delta/\lambda \ll 1$), and the other limit where lattice distortions dominate ($\Delta/\lambda \gg 1$). For these limits, we find

$$\lim_{\Delta/\lambda\to 0} \tan\theta = \frac{1}{\sqrt{2}} \qquad \text{and} \qquad \lim_{\Delta/\lambda\to\pm\infty} \tan\theta = -\frac{\lambda}{\sqrt{2}\Delta}. \quad (6.4)$$

The ground state of the Ir ion is doubly degenerate in both cases. When lattice distortions are absent, $J_{\rm eff}$ is a good quantum number and the g and h doublets together form the $J_{\rm eff} = 3/2$ quartet, while the hole occupies the f doublet with $J_{\rm eff} = 1/2$ [Eq. (6.1) has $\sin\theta = \sqrt{1/3}$ and $\cos\theta = \sqrt{2/3}$ in this limit]. The

energies become $E_f = \lambda$ and $E_g = E_h = -\lambda/2$, as noted above. When lattice distortions dominate, $\theta \to 0$. The hole occupies the h doublet, which becomes $\{|xy\uparrow\rangle, |xy\downarrow\rangle\}$. The energies of the doublets in this limit are $E_f = E_g = -\Delta$ and $E_h = 0$.

The RIXS experiments proposed in this chapter enable one to distinguish between the two scenario's, and so can provide complimentary evidence to existing data. But from RIXS data, one could draw more conclusions since one can probe the excitation spectrum. In the remainder of this section, the excitation spectrum of Sr_2IrO_4 is discussed.

Collective behavior of the *f* doublet. When spin-orbit coupling dominates, Sr_2IrO_4's excitation spectrum of the f doublet is quite remarkable: the $J_{\text{eff}} = 1/2$ levels interact via superexchange and the low energy effective Hamiltonian is of Heisenberg form, as described in, for instance, Ref. [214]. We briefly review this Hamiltonian here. Starting from the spin-orbital superexchange Hamiltonian for 1 electron in the triply degenerate t_{2g} orbitals (Eq. (3.11) from Ref. [160]), one projects on the low energy Kramers doublet and obtains a low energy effective superexchange Hamiltonian for these pseudo-spin-1/2 states:

$$H_{\text{eff}} = J_1 \tilde{\mathbf{S}}_i \cdot \tilde{\mathbf{S}}_j + J_2 (\tilde{\mathbf{S}}_i \cdot \mathbf{r}_{ij})(\mathbf{r}_{ij} \cdot \tilde{\mathbf{S}}_j) \tag{6.5}$$

where $\tilde{\mathbf{S}}$ is the pseudo-spin-1/2 operator, $\mathbf{r}_{ij}$ is the unit vector directed along the ij bond, and $J_{1,2}$ are energies determined by Hund's rule coupling J_H. For $J_H \ll U$, we get $J_1 \approx 4/9$ and $J_2 \approx 2J_H/9U$ in units of $4t^2/U$, with t the Ir-Ir hopping integral and U the same-orbital Coulomb repulsion. In this limit, the result is a Heisenberg coupling with weak dipolar anisotropy [214].

Next, the rotation of the octahedra (by an angle $\alpha \approx 11^\circ$) are taken into account, resulting in a Dzyaloshinsky-Moriya (DM) interaction. The DM interaction rotates the spins by an angle $\phi \approx 8^\circ$. The difference between α and ϕ is controlled by the distortion along the z axis. In the limit of no distortion along the z axis, $\alpha = \phi$. The Hamiltonian on the bond ij with $J_H = 0$ but non-zero DM interaction is

$$H_{ij} = J\tilde{\mathbf{S}}_i \cdot \tilde{\mathbf{S}}_j + J_z \tilde{S}_i^z \tilde{S}_j^z + \mathbf{D} \cdot \tilde{\mathbf{S}}_i \times \tilde{\mathbf{S}}_j \tag{6.6}$$

where $\mathbf{D} = (0, 0, -D)$ (which flips sign on alternating bonds) and the energies J, J_z and D are defined in terms of the octahedron rotation angle α and the distortion parameter θ as in Ref. [214]. The DM interaction term can be transformed away by rotating the spin operators around the z axis over the spin canting angle $\pm\phi$ (alternating with sublattice) with $\tan 2\phi = -D/J$. We define the unitary transformation $U(\phi) = \otimes_i \exp\{-i(\pm 1)^i \phi S_i^z\}$ where $(\pm)^i = 1$ on the sublattice A, where the octahedron are rotated over $+\alpha$, and -1 on sublattice B $(-\alpha)$. The transformed Hamiltonian is

$$\tilde{H} = U(\phi) H U^{-1}(\phi) = \tilde{J}\tilde{\mathbf{S}}_i \cdot \tilde{\mathbf{S}}_j, \tag{6.7}$$

where $\tilde{J} = J + J_z$. Note that the isotropic form is only retreived when there is a special relation between J, J_z and D. When $J_H/U = 0$, the degeneracy of the ground state is not lifted by the DM interaction[1]. A more extended version including Hund's rule exchange is given in Ref. [214].

It is remarkable that Sr_2IrO_4 is not only structurally identical to La_2CuO_4, it also has the same low energy excitation spectrum. However, the physical form and origin of these excitations are are not at all similar.

Local behavior of the *g* and *h* doublets. Excitations to the g and h doublets are very interesting because it is conjectured that Sr_2IrO_4 is a Mott insulator only because of the large spin-orbit coupling [222,224]. The $J_{\text{eff}} = 1/2$ doublet consists of small orbitals, which have small hopping amplitudes, therefore confining the charges and making the system Mott insulating. The $J_{\text{eff}=3/2}$ quartet consists of larger orbitals with larger hopping amplitudes, which would perhaps be enough to form metallic bands. If that picture is correct, then the g and h excitations should be very broad in RIXS: the excited electrons come from all the occupied g and h bands, and the spectrum is a convolution over all these widely dispersing states. In contrast, if Sr_2IrO_4 is a conventional Mott insulator, the g and h excitations will be localized and have more sharply defined energies. Since J is small compared to λ, these excitations will disperse very little. They have an energy slightly larger than the Mott gap, and decay via electron-hole pairs reduces their lifetime. Also, superexchange processes will often result in decay to $J_{\text{eff}} = 1/2$ states. In practice, this will make it very hard to distinguish between the two theories for the insulating behavior. On the other hand, the coupling of the inter-spin-orbit multiplet excitations to charge modes enables RIXS to also probe the latter.

6.3 Iridium L edge cross section

The spin-orbital degrees of freedom can be probed with direct RIXS at the Ir L edge. This process involves two (dipole) transitions connecting the 2p core states to the 5d valence ones. Here, we consider the case that the incident photons are tuned to excite a core electron into the empty t_{2g} state.

The intermediate state (5d t_{2g}^6) has a filled shell. The dominant multiplet effect comes from the core orbital's spin-orbit coupling Λ: the 2p core states split into $J = 1/2$ (the L_2 edge) and $J = 3/2$ states (the L_3 edge), like at the Cu L edge. Since the L_2 and L_3 edge are separated by 1.6 keV [223], their interfere is negligible, given the much smaller lifetime broadening (a few eV [100]).

[1] This can be understood as follows: the $J_{\text{eff}} = 1/2$ Kramers doublet states are each others' time-reversed states. This implies that their charge distributions are the same, and therefore also the hopping amplitudes to the neighboring oxygens (possibly up to a sign, although this sign cannot be affected by a continous rotation of the octahedra). By symmetry, rotation of the octahedra does not change the equality of the hopping amplitudes. This means there cannot be a preferential state and preferential direction, and thus no anisotropy.

The lifetime broadening at the Ir L edge is still quite large compared to the dynamics of the 5d electrons. Therefore, the UCL expansion should work quite well. We employ the UCL expansion to zeroth order. To obtain the cross section, one only needs the dipole operators.

6.3.1 Dipole operators

We introduce the electron annihilation operators for the 2p orbital angular momentum eigenstates

$$\begin{aligned} p_x &= -\tfrac{1}{\sqrt{2}}(p_1 - p_{-1}) \\ p_y &= \tfrac{i}{\sqrt{2}}(p_1 + p_{-1}) \\ p_z &= p_0, \end{aligned} \tag{6.8}$$

analogous to Eqs. (6.2). The core electron eigenstates are easily obtained from Sec. 6.2, because both the valence and the core electrons are spin-orbit coupled and have orbital angular momentum 1. The $J = 1/2$ states are lowest in energy, which means that the L_2 edge is higher in energy than the L_3 edge. In analogy to the valence electrons, we introduce the 2p electron annihilation operators $F_{\uparrow,\downarrow}$ for the L_2 wave functions and $G_{\uparrow,\downarrow}, H_{\uparrow,\downarrow}$ for the L_3 ones. For symmetry of notation, we introduce a tetragonal distortion δ for the core levels too, which splits the $J = 3/2$ quartet into two doublets G and H. We find, in analogy to Eqs. (6.3),

$$\begin{aligned} F_\uparrow &= \sin\Theta\ p_{0\uparrow} - \cos\Theta\ p_{1\downarrow}, \qquad & G_\uparrow &= p_{1\uparrow}, \qquad & H_\uparrow &= \cos\Theta\ p_{0\uparrow} + \sin\Theta\ p_{1\downarrow}, \\ F_\downarrow &= \sin\Theta\ p_{0\downarrow} - \cos\Theta\ p_{-1\uparrow}, & G_\downarrow &= p_{-1\downarrow}, & H_\downarrow &= \cos\Theta\ p_{0\downarrow} + \sin\Theta\ p_{-1\uparrow}, \end{aligned} \tag{6.9}$$

where $\tan 2\Theta = 2\sqrt{2}\Lambda/(\Lambda - 2\delta)$.

Now, we calculate the dipole matrix elements for the Ir L edge. We write the dipole operator in second quantization ($p_x^\dagger$ creates a $2p_x$ electron, $d_{xy}^\dagger$ creates a $5d_{xy}$ electron, etc.), and use the octahedral symmetry of Sr_2IrO_4 to simplify the expression:

$$\begin{aligned} \mathbf{x}\cdot\boldsymbol{\epsilon} &= \sum_{i,j,k,\sigma} d_{k\sigma}^\dagger \langle 5d_k|\, x_i\, |2p_j\rangle\, \epsilon_i p_{j\sigma} + \text{h.c.} \\ &= \sum_\sigma d_{yz\sigma}^\dagger \langle 5d_{yz}| \left(y\,|2p_z\rangle\, \epsilon_y p_{z\sigma} + z\,|2p_y\rangle\, \epsilon_z p_{y\sigma} \right) + ..zx.. + ..xy.. + \text{h.c.} \\ &= -i\,\langle 5d_{yz}|\, y\,|2p_z\rangle \sum_\sigma \Big[\epsilon_+ (d_{-1}^\dagger p_0 - d_0^\dagger p_1) + \epsilon_- (d_1^\dagger p_0 - d_0^\dagger p_{-1}) \\ &\quad + \epsilon_z (d_1^\dagger p_{-1} - d_{-1}^\dagger p_1) \Big] + \text{h.c.} = (D_2 + D_3) + \text{h.c.} \end{aligned} \tag{6.10}$$

where $\epsilon_\pm = (\epsilon_x \pm i\epsilon_y)/\sqrt{2}$, and the spin label σ is suppressed in the last lines but implied for every electron operator. The dipole operators for the L_2 and L_3

edge, respectively, are

$$\begin{aligned} D_2 = -i \langle 5d_{yz}| y |2p_z\rangle \Big[& \epsilon_+ \left(\left\{ (ss'+cc')h_\downarrow^\dagger + (sc'-cs')f_\downarrow^\dagger \right\} F_\uparrow + s' g_\downarrow^\dagger F_\downarrow \right) \\ & + \epsilon_- \left(\left\{ (ss'+cc')h_\uparrow^\dagger + (sc'-cs')f_\uparrow^\dagger \right\} F_\downarrow + s' g_\uparrow^\dagger F_\uparrow \right) \\ & + \epsilon_z c' \left(g_\downarrow^\dagger F_\uparrow - g_\uparrow^\dagger F_\downarrow \right) \Big], \end{aligned} \tag{6.11}$$

$$\begin{aligned} D_3 = -i \langle 5d_{yz}| y |2p_z\rangle \Big[& \epsilon_+ \left(c' g_\downarrow^\dagger H_\downarrow + \left\{ (sc'-cs')h_\downarrow^\dagger - (ss'+cc')f_\downarrow^\dagger \right\} H_\uparrow \right. \\ & \left. - \left\{ s f_\uparrow^\dagger + c h_\uparrow^\dagger \right\} G_\uparrow \right) + \epsilon_- \left(c' g_\uparrow^\dagger H_\uparrow + \left\{ (sc'-cs')h_\uparrow^\dagger - (ss'+cc')f_\uparrow^\dagger \right\} H_\downarrow \right. \\ & \left. - \left\{ s f_\downarrow^\dagger + c h_\downarrow^\dagger \right\} G_\downarrow \right) + \epsilon_z \left(s' g_\uparrow^\dagger H_\downarrow + \left\{ s h_\uparrow^\dagger - c f_\uparrow^\dagger \right\} G_\downarrow - \left\{ s h_\downarrow^\dagger - c f_\downarrow^\dagger \right\} G_\uparrow \right. \\ & \left. - s' g_\downarrow^\dagger H_\uparrow \right) \Big] \end{aligned} \tag{6.12}$$

where we abbreviated $\sin\Theta = s'$ and $\sin\theta = s$ (and similar for the cosines).

6.3.2 Local RIXS scattering operator

The expressions for the dipole operators at the $L_{2,3}$ edges [Eqs. (6.11) and (6.12)] can be inserted in Eq. (2.41), and give, to zeroth order in the UCL expansion,

$$\mathcal{F}_{fi} = \frac{1}{i\Gamma} \sum_i e^{i\mathbf{q}\cdot\mathbf{R}_i} \langle f| (D_{2,3}^\dagger)_i (D_{2,3})_i |i\rangle \tag{6.13}$$

We define the single site RIXS scattering operators $O_{2,3} = D_{2,3}^\dagger D_{2,3}$ (the site index is suppressed in the following). Projecting out the core hole degrees of freedom, these become

$$\begin{aligned} O_2 = \sin(\theta-\Theta) \sum_{\sigma\in\{\uparrow,\downarrow\}} \Big[& \epsilon'^*_{\bar\sigma} \epsilon_{\bar\sigma} \sin(\theta-\Theta) f_\sigma f_\sigma^\dagger + \epsilon'^*_\sigma \epsilon_{\bar\sigma} s' g_{\bar\sigma} f_\sigma^\dagger \\ & - (-1)^\sigma \epsilon'^*_z \epsilon_{\bar\sigma} c' g_\sigma f_\sigma^\dagger + \epsilon'^*_{\bar\sigma} \epsilon_{\bar\sigma} \cos(\theta-\Theta) h_\sigma f_\sigma^\dagger \Big] \end{aligned} \tag{6.14}$$

at the L_2 edge. The factor $|\langle 5d_{yz}| y |2p_z\rangle|^2$, which is just a positive number, is dropped. We define $(-1)^\sigma$ to be 1 for $\sigma = \uparrow$ and -1 for $\sigma = \downarrow$. Further, $\epsilon_\uparrow = \epsilon_+$ and $\epsilon_\downarrow = \epsilon_-$. Note that $\epsilon'^*_+ = (\epsilon'_x + i\epsilon'_y)^*/\sqrt{2}$. For the L_3 edge,

$$O_3 = \sum_{\sigma\in\{\uparrow,\downarrow\}} \Big[\left\{ \epsilon'^*_\sigma \epsilon_\sigma s^2 + \epsilon'^*_{\bar\sigma} \epsilon_{\bar\sigma} \cos^2(\theta-\Theta) + \epsilon'^*_z \epsilon_z c^2 \right\} f_\sigma f_\sigma^\dagger +$$

$$
\begin{aligned}
&+ \left\{(-1)^{\sigma}(\epsilon'^{*}_{\bar{\sigma}}\epsilon_z - \epsilon'^{*}_{z}\epsilon_{\sigma})sc\right\} f_{\bar{\sigma}}f^{\dagger}_{\sigma} \\
&- \left\{(-1)^{\sigma}\epsilon'^{*}_{z}\epsilon_{\bar{\sigma}}s'\cos(\theta-\Theta)\right\} g_{\sigma}f^{\dagger}_{\sigma} - \epsilon'^{*}_{\sigma}\epsilon_{\bar{\sigma}}c'\cos(\theta-\Theta)g_{\bar{\sigma}}f^{\dagger}_{\sigma} \\
&+ \left\{(\epsilon'^{*}_{\sigma}\epsilon_{\sigma} - \epsilon'^{*}_{z}\epsilon_{z})\frac{1}{2}\sin 2\theta - \epsilon'^{*}_{\bar{\sigma}}\epsilon_{\bar{\sigma}}\frac{1}{2}\sin 2(\theta-\Theta)\right\} h_{\sigma}f^{\dagger}_{\sigma} \\
&+ \left\{(-1)^{\sigma}(\epsilon'^{*}_{z}\epsilon_{\sigma}s^2 + \epsilon'^{*}_{\bar{\sigma}}\epsilon_z c^2)\right\} h_{\bar{\sigma}}f^{\dagger}_{\sigma}\Big] .
\end{aligned} \tag{6.15}
$$

When spin-orbit coupling dominates, $\theta = \Theta$ and the inelastic scattering intensity at the L_2 edge completely vanishes, in addition to the vanishing elastic intensity [223]. In the presence of a large crystal field, this no longer holds: the core electrons are much less affected by the crystal field than the 5d ones. In the following, we split the local scattering operator into three parts that create excitations in the f, g and h doublets.

Excitations within the *f* doublet. When $\lambda \gg \Delta$, excitations within the $J_{\text{eff}} = 1/2$ doublet are lowest in energy. The single site RIXS scattering operator for intra-f doublet excitations can be written in terms of Pauli matrices that act on the pseudo-spin of the f fermion. At the L_2 edge,

$$
O_2^{(f)} = \frac{1}{2}\sin^2(\theta-\Theta)\left[\left(P_{A_{1g}} + \frac{1}{\sqrt{3}}Q_3\right)\mathbb{1}_2 - P_z\sigma_z\right], \tag{6.16}
$$

and at the L_3 edge

$$
\begin{aligned}
O_3^{(f)} = &\left[\frac{1}{6}\cos^2(\theta-\Theta)\left(3P_{A_{1g}} + \sqrt{3}Q_3\right) + \frac{3}{2}P_{A_{1g}} - \frac{\sqrt{3}}{6}(2c^2-s^2)Q_3\right]\mathbb{1}_2 \\
&- \frac{1}{2}\left(\cos^2(\theta-\Theta) - s^2\right)P_z\sigma_z + \frac{\sin 2\theta}{2\sqrt{2}}(P_x\sigma_x + P_y\sigma_y),
\end{aligned} \tag{6.17}
$$

where we introduced polarization factors

$$
\begin{aligned}
P_x &= i\left(\epsilon'^{*}_{y}\epsilon_z - \epsilon'^{*}_{z}\epsilon_y\right), \quad T_x = \epsilon'^{*}_{y}\epsilon_z + \epsilon'^{*}_{z}\epsilon_y, \quad P_{A_{1g}} = \tfrac{2}{3}\left(\epsilon'^{*}_{x}\epsilon_x + \epsilon'^{*}_{y}\epsilon_y + \epsilon'^{*}_{z}\epsilon_z\right), \\
P_y &= i\left(\epsilon'^{*}_{z}\epsilon_x - \epsilon'^{*}_{x}\epsilon_z\right), \quad T_y = \epsilon'^{*}_{x}\epsilon_z + \epsilon'^{*}_{z}\epsilon_x, \quad Q_2 = \epsilon'^{*}_{y}\epsilon_y - \epsilon'^{*}_{x}\epsilon_x, \\
P_z &= i\left(\epsilon'^{*}_{x}\epsilon_y - \epsilon'^{*}_{y}\epsilon_x\right), \quad T_z = \epsilon'^{*}_{x}\epsilon_y + \epsilon'^{*}_{y}\epsilon_x, \quad Q_3 = \tfrac{1}{\sqrt{3}}\left(\epsilon'^{*}_{x}\epsilon_x + \epsilon'^{*}_{y}\epsilon_y - 2\epsilon'^{*}_{z}\epsilon_z\right).
\end{aligned} \tag{6.18}
$$

The polarization factors are chosen such that they are normalized as $\mathrm{Tr}(\Gamma^2) = 2$, where the matrices Γ are defined by the polarization factors P as $P = \epsilon'^{*}_i\Gamma_{ij}\epsilon_j$.

In the cubic limit, O_2 vanishes, while at the L_3 edge one finds

$$
O_3^{(f)} = P_{A_{1g}}\mathbb{1}_2 + \frac{1}{3}(P_x\sigma_x + P_y\sigma_y - P_z\sigma_z). \tag{6.19}
$$

This is not a scalar product, which might be surprising because of the octahedral symmetry. However, the 5d t_{2g} orbitals do not transform as a vector: they have

effective angular momentum $\mathbf{l} = -\mathbf{L}$. The Zeeman energy $\mathbf{B}\cdot\mathbf{S}$, projected on the f doublet, transforms in a similar way:

$$\mathbf{B}\cdot\mathbf{S} = \cos 2\theta\ B_z\sigma_z - s^2(B_x\sigma_x + B_y\sigma_y) \xrightarrow{\Delta\to 0} -\frac{1}{3}\left(B_x\sigma_x + B_y\sigma_y - B_z\sigma_z\right) \quad (6.20)$$

These combinations become scalar products when we flip the sign of either $f_\uparrow$ or $f_\downarrow$ in Eq. (6.3). Note that the Hamiltonians (6.5) and (6.6) are invariant under such a sign change. In the following, we will flip the sign of $f_\downarrow$. The inelastic parts of the scattering operators become

$$O_2^{(f)} \xrightarrow{\Delta\to 0} 0, \quad (6.21)$$

$$O_3^{(f)} \xrightarrow{\Delta\to 0} -\frac{1}{3}\left(P_x\sigma_x + P_y\sigma_y + P_z\sigma_z\right). \quad (6.22)$$

Excitation of g and h doublets. For the L_2 edge,

$$O_2^{(g)} = \sin(\theta-\Theta)\left[\frac{is'}{2}\left(Q_2\sigma_y^{(g)} + T_z\sigma_x^{(g)}\right) - \frac{c'}{2\sqrt{2}}(T_y - iP_y)\mathbb{1}_2^{(g)} + \frac{ic'}{2\sqrt{2}}(T_x + iP_x)\sigma_z^{(g)}\right], \quad (6.23)$$

$$O_2^{(h)} = \frac{1}{4}\sin 2(\theta-\Theta)\left[\left(P_{A_{1g}} + \tfrac{1}{\sqrt{3}}Q_3\right)\sigma_z^{(h)} - P_z\,\mathbb{1}_2^{(h)}\right], \quad (6.24)$$

where, for instance, $\sigma_z^{(h)} = h_\uparrow f_\uparrow^\dagger - h_\downarrow f_\downarrow^\dagger$, and where the sign flip on $f_\downarrow$ discussed above is incorporated.

At the L_3 edge,

$$O_3^{(g)} = \cos(\theta-\Theta)\left[-\frac{s'}{2\sqrt{2}}(T_y - iP_y)\mathbb{1}_2^{(g)} + \frac{is'}{2\sqrt{2}}(T_x + iP_x)\sigma_z^{(g)} - \frac{ic'}{2}Q_2\sigma_y^{(g)} + \frac{ic'}{2}T_z\sigma_x^{(g)}\right], \quad (6.25)$$

$$O_3^{(h)} = \frac{1}{4}\left[\sqrt{3}\sin 2\theta\ Q_3 - \sin 2(\theta-\Theta)\left(P_{A_{1g}} + \tfrac{1}{\sqrt{3}}Q_3\right)\right]\sigma_z^{(h)} + \frac{i}{4}\left[\sin 2\theta + \sin 2(\theta-\Theta)\right]P_z\mathbb{1}_2^{(h)} + \frac{1}{2\sqrt{2}}\left[T_y + i\cos 2\theta\ P_y\right]\sigma_x^{(h)} + \frac{1}{2\sqrt{2}}\left[T_x - i\cos 2\theta\ P_x\right]\sigma_y^{(h)}. \quad (6.26)$$

In the cubic limit, one obtains

$$O_2^{(g)} = O_2^{(h)} = 0 \quad (6.27)$$

$$O_3^{(g)} = \frac{1}{\sqrt{6}}\left[-\frac{1}{2}(T_y - iP_y)\mathbb{1}_2^{(g)} + \frac{i}{2}(T_x + iP_x)\sigma_z^{(g)} - iQ_2\sigma_y^{(g)} + iT_z\sigma_x^{(g)}\right] \quad (6.28)$$

$$O_3^{(h)} = \frac{1}{3\sqrt{2}}\left[iP_z\mathbb{1}_2^{(h)} + \sqrt{3}Q_3\sigma_z^{(h)} + \frac{3}{2}\left(T_y\sigma_x^{(h)} + T_x\sigma_y^{(h)}\right) + \frac{i}{2}\left(P_y\sigma_x^{(h)} - P_x\sigma_y^{(h)}\right)\right]. \quad (6.29)$$

6.3.3 Iridium L edge RIXS cross section

Up to this point, the discussion is general and applies to all materials with an Ir^{4+} ion in an octahedral crystal field, including Kitaev-Heisenberg model compounds. To obtain the RIXS cross sections for a certain material from the scattering operators $O_{2,3}$ is straightforward once the Hamilonian governing the interactions between the Ir ions in that material is given.

In the remainder of this chapter, we specify to the case of Sr_2IrO_4. As laid out in Sec. 6.2, we distinguish between the low energy Kramers doublet, which shows collective behavior in the limit of strong spin-orbit coupling, and the high energy quartet, which does not.

Cross section of intra- *f* doublet excitations. It should be noted that the local scattering operators $O_{2,3}$ are derived in the local axes of a rotated octahedron. The Hamiltonian (6.6), however, is written in global coordinates. Therefore, the polarization and spin vectors should be rotated back over an angle α to obtain the scattering operator in global coordinates too. Reserving primes for the local axes, one gets

$$\begin{aligned}
P'_x &= \cos\alpha\ P_x + \sin\alpha\ P_y, & T'_x &= \cos\alpha\ T_x - \sin\alpha\ T_y,\\
P'_y &= \cos\alpha\ P_y - \sin\alpha\ P_x, & T'_y &= \cos\alpha\ T_y + \sin\alpha\ T_x,\\
P'_z &= P_z, & T'_z &= \sin 2\alpha\ Q_2 + \cos 2\alpha\ T_z,\\
Q'_2 &= \cos 2\alpha\ Q_2 - \sin 2\alpha\ T_z, & Q'_3 &= Q_3, \qquad P'_{A_{1g}} = P_{A_{1g}},
\end{aligned} \quad (6.30)$$

for the polarization factors. α flips sign on sublattice B, which is rotated in the opposite direction. The rotated spin operators are

$$\begin{aligned}
S_i'^x &= U(-\alpha)S^xU^{-1}(-\alpha) = \cos\alpha\ S^x - (\pm 1)^i \sin\alpha\ S^y,\\
S_i'^y &= U(-\alpha)S^yU^{-1}(-\alpha) = \cos\alpha\ S^y + (\pm 1)^i \sin\alpha\ S^x,\\
S_i'^z &= U(-\alpha)S^zU^{-1}(-\alpha) = S_i^z,
\end{aligned} \quad (6.31)$$

where $(\pm 1)^i$ is 1 on sublattice A and -1 on sublattice B. After this rotation, the spins are transformed by $U(\phi)$ to the basis in which the Hamiltonian is of Heisenberg type. Since $\alpha \approx \phi$, the unitary transformation nearly cancels the rotation over α. For $\alpha = \phi$, the cancellation is complete. In the following, we

work in the cubic limit, so $\alpha = \phi$, and obtain for the complete, multi-site, inelastic scattering operator:

$$O_{\mathbf{q}} = \sum_i e^{i\mathbf{q}\cdot\mathbf{R}_i}(O_3^{(f)})_i = -\frac{1}{3}\sum_i \Big[\sin\alpha\; e^{i(\mathbf{q}+\mathbf{Q})\cdot\mathbf{R}_i}\,(P_y\sigma_x - P_x\sigma_y) + e^{i\mathbf{q}\cdot\mathbf{R}_i}\,(\cos\alpha\,\{P_x\sigma_x + P_y\sigma_y\} + P_z\sigma_z)\Big] \tag{6.32}$$

where $\mathbf{Q} = (\pi, \pi)$. Following Eq. (6.13), the RIXS cross section is then

$$\frac{d^2\sigma}{d\Omega d\omega} \propto \sum_f |\langle f|\, O_{\mathbf{q}}\, |g\rangle|^2\, \delta(\hbar\omega - \hbar\omega_f), \tag{6.33}$$

where $\hbar\omega_f$ is the energy of the final state $|f\rangle$.

To describe the pseudo-spin flip excitation spectrum of the pseudo-spin Heisenberg model, Holstein-Primakoff bosons are introduced, in analogy to the magnetic Heisenberg model in Sec. 4.2. The reference state is taken to be the Néel state with ordering direction [110] [223], and accordingly, the vectors $\hat{\mathbf{n}}_1 = (-1,1,0)/\sqrt{2},\ \hat{\mathbf{n}}_2 = (0,0,1),\ \hat{\mathbf{n}}_3 = (1,1,0)/\sqrt{2}$ are introduced. The scattering operator becomes

$$O_{\mathbf{q}} = -\frac{1}{3}\sum_i \left[\frac{\sin\alpha}{\sqrt{2}} e^{i(\mathbf{q}+\mathbf{Q})\cdot\mathbf{R}_i}\,\{(P_y - P_x)\hat{\mathbf{n}}_3\cdot\boldsymbol{\sigma}_i - (P_x + P_y)\hat{\mathbf{n}}_1\cdot\boldsymbol{\sigma}_i\} + e^{i\mathbf{q}\cdot\mathbf{R}_i}\left(\frac{\cos\alpha}{\sqrt{2}}\{(P_x + P_y)\hat{\mathbf{n}}_3\cdot\boldsymbol{\sigma}_i + (P_y - P_x)\hat{\mathbf{n}}_1\cdot\boldsymbol{\sigma}_i\} + P_z\hat{\mathbf{n}}_2\cdot\boldsymbol{\sigma}_i\right)\right]. \tag{6.34}$$

The Holstein-Primakoff bosons are naturally introduced in the new coordinate frame spanned by $\hat{\mathbf{n}}_1, \hat{\mathbf{n}}_2$ and $\hat{\mathbf{n}}_3$:

$$\sum_i e^{i\mathbf{q}\cdot\mathbf{R}_i}\hat{\mathbf{n}}_1\cdot\boldsymbol{\sigma}_i = \sqrt{N}(u_{\mathbf{q}} - v_{\mathbf{q}})(\alpha^\dagger_{\mathbf{q}} + \alpha_{-\mathbf{q}}) \tag{6.35}$$

$$\sum_i e^{i\mathbf{q}\cdot\mathbf{R}_i}\hat{\mathbf{n}}_2\cdot\boldsymbol{\sigma}_i = i\sqrt{N}(u_{\mathbf{q}} - v_{\mathbf{q}})(\alpha^\dagger_{\mathbf{q}+\mathbf{Q}} - \alpha_{-\mathbf{q}-\mathbf{Q}}) \tag{6.36}$$

$$\sum_i e^{i\mathbf{q}\cdot\mathbf{R}_i}\hat{\mathbf{n}}_3\cdot\boldsymbol{\sigma}_i = \delta_{\mathbf{q},\mathbf{Q}}\left(N - 2\sum_{\mathbf{k}} v^2_{\mathbf{k}}\right) + 2\sum_{\mathbf{k}}\Big[u_{\mathbf{k}+\mathbf{q}}v_{\mathbf{k}}\left(\alpha^\dagger_{\mathbf{k}+\mathbf{q}+\mathbf{Q}}\alpha^\dagger_{-\mathbf{k}} + \alpha_{\mathbf{k}}\alpha_{-\mathbf{k}-\mathbf{q}-\mathbf{Q}}\right) + (v_{\mathbf{k}}v_{\mathbf{k}+\mathbf{q}} - u_{\mathbf{k}}u_{\mathbf{k}+\mathbf{q}})\alpha^\dagger_{\mathbf{k}+\mathbf{q}+\mathbf{Q}}\alpha_{\mathbf{k}}\Big] \tag{6.37}$$

with $u_{\mathbf{k}}$ and $v_{\mathbf{k}}$ defined as in Eq. (4.10). The ground state is approximated by the (pseudo-)magnon vacuum $|0\rangle$. The scattering operator consists of a single-

magnon part

$$O_{\mathbf{q}}^{(1)} = \frac{\sqrt{N}}{3}\left[\frac{\sin\alpha}{\sqrt{2}}(P_x+P_y)(u_{\mathbf{q}}+v_{\mathbf{q}})\left(\alpha^{\dagger}_{\mathbf{q}+\mathbf{Q}}+\alpha_{-\mathbf{q}-\mathbf{Q}}\right)\right.$$
$$+\frac{\cos\alpha}{\sqrt{2}}(P_x-P_y)(u_{\mathbf{q}}-v_{\mathbf{q}})\left(\alpha^{\dagger}_{\mathbf{q}}+\alpha_{-\mathbf{q}}\right)$$
$$\left.-iP_z(u_{\mathbf{q}}-v_{\mathbf{q}})\left(\alpha^{\dagger}_{\mathbf{q}+\mathbf{Q}}-\alpha_{-\mathbf{q}-\mathbf{Q}}\right)\right] \tag{6.38}$$

and a double-magnon part

$$O_{\mathbf{q}}^{(2)} = -\frac{\sqrt{2}}{3}\sum_{\mathbf{k}} u_{\mathbf{k}+\mathbf{q}}v_{\mathbf{k}}\left[\sin\alpha\ (P_y-P_x)\left(\alpha^{\dagger}_{\mathbf{k}+\mathbf{q}}\alpha^{\dagger}_{-\mathbf{k}}+\alpha_{\mathbf{k}}\alpha_{-\mathbf{k}-\mathbf{q}}\right)\right.$$
$$\left.+\cos\alpha\ (P_x+P_y)\left(\alpha^{\dagger}_{\mathbf{k}+\mathbf{q}+\mathbf{Q}}\alpha^{\dagger}_{-\mathbf{k}}+\alpha_{\mathbf{k}}\alpha_{-\mathbf{k}-\mathbf{q}-\mathbf{Q}}\right)\right]. \tag{6.39}$$

The part of the scattering operator that does not change the number of magnons is not considered here.

The single-magnon intensity then becomes

$$I^{(1)} \propto \frac{N}{9}\left[\left|\frac{\sin\alpha}{\sqrt{2}}(P_x+P_y)(u_{\mathbf{q}}+v_{\mathbf{q}})-iP_z(u_{\mathbf{q}}-v_{\mathbf{q}})\right|^2\right.$$
$$\left.+\frac{1}{2}\cos^2\alpha\ \left|P_x-P_y\right|^2(u_{\mathbf{q}}-v_{\mathbf{q}})^2\right]\delta(\omega-\omega_{\mathbf{q}}), \tag{6.40}$$

and the two-magnon intensity

$$I^{(2)} \propto \frac{2}{9}\sum_{\mathbf{k}}\left[\sin^2\alpha\left|P_x-P_y\right|^2(u_{\mathbf{k}+\mathbf{q}}v_{\mathbf{k}}+u_{\mathbf{k}}v_{\mathbf{k}+\mathbf{q}})^2\right.$$
$$\left.+\cos^2\alpha\left|P_x+P_y\right|^2(u_{\mathbf{k}+\mathbf{q}}v_{\mathbf{k}}-u_{\mathbf{k}}v_{\mathbf{k}+\mathbf{q}})^2\right]\delta(\omega-\omega_{\mathbf{k}+\mathbf{q}}-\omega_{\mathbf{k}}). \tag{6.41}$$

Note that for non-zero α there will be single-magnon weight at $\mathbf{q}=\mathbf{0}$, in contrast to our calculations for the cuprates, where the rotation of the octahedra was not included.

Cross section of *g* and *h* excitations. For the g and h excitations, one only has to consider the polarization dependence, because in a Mott insulating state there is no collective behavior expected. The excitations decay rapidly via particle-hole excitations and through superexchange coupling to, amongst others, the f doublet on neighboring sites. Rapid decay eliminates collective behavior, and therefore all $\mathbf{q}$ dependence. In a metallic state, the g and h excitations will be broad convolutions over the bands they form, and are thus also $\mathbf{q}$-independent. Both excitations will be broadened quite strongly.

For local excitations, it is convenient to express the RIXS intensity in terms of Green's functions:

$$I \propto \sum_f |\langle f| O_{\mathbf{q}} |g\rangle|^2 \, \delta(\omega - \omega_{fi}) = -\frac{1}{\pi} \mathfrak{Im} \{G_{\mathbf{q}}(\omega)\} \tag{6.42}$$

with

$$G_{\mathbf{q}}(\omega) = -i \int_0^\infty dt e^{i\omega t} \langle g| O_{\mathbf{q}}^\dagger(t) O_{\mathbf{q}}(0) |g\rangle \,, \tag{6.43}$$

where $|g\rangle$ is the ground state. In the case of local excitations, $G(\omega)$ is a quite simple quantity. For instance, for g excitations one gets

$$G_{\mathbf{q}}^{(g)}(\omega) = -i \int_0^\infty dt e^{i(\omega-\omega_g)t} \langle g| \sum_j e^{-i\mathbf{q}\cdot\mathbf{R}_j} O_j^\dagger \sum_i e^{i\mathbf{q}\cdot\mathbf{R}_i} O_i \, |g\rangle \tag{6.44}$$

$$= \lim_{\eta\to 0} \frac{1}{\omega - \omega_g + i\eta} \sum_i \langle g| O_i^\dagger O_i \, |g\rangle \tag{6.45}$$

where $\hbar\omega_g = \lambda/\sqrt{2}\tan\theta - (-\Delta - \lambda/2)$ (the energy splitting between the local ground state and a hole in the g states). We also define $\hbar\omega_h = \lambda/\sqrt{2}\tan\theta - (-\lambda\tan\theta)/\sqrt{2}$ for the h excitations. For simplicity, we have neglected the superexchange coupling for the f states so that the energy of the g and h excitations are given by the local considerations of Sec. 6.2, i.e., without corrections for the broken superexchange bonds between neighboring f holes, etc. Also, we neglect the rotation of the octahedra.

We note that

$$\begin{aligned}
&\langle g| \mathbb{1}_2^{(g,h)\dagger} \mathbb{1}_2^{(g,h)} |g\rangle = \langle g| \sigma_a^{(g,h)\dagger} \sigma_a^{(g,h)} |g\rangle = \langle g| \mathbb{1}_2^{(f)} |g\rangle \,, \\
&\langle g| \sigma_a^{(g,h)\dagger} \sigma_b^{(g,h)} |g\rangle = i\epsilon_{abc} \langle g| \sigma_c^{(f)} |g\rangle = 0, \\
&\langle g| \mathbb{1}_2^{(g,h)\dagger} \sigma_a^{(g,h)} |g\rangle = \langle g| \sigma_a^{(f)} |g\rangle = 0,
\end{aligned} \tag{6.46}$$

where $\{a,b,c\} = \{x,y,z\}$ and $\sigma_z^{(f)} = f_\uparrow f_\uparrow^\dagger - f_\downarrow f_\downarrow^\dagger$ etc. Writing the scattering operator as the inner product $(A_0, A_1, A_2, A_3) \cdot (\mathbb{1}_2^{(g,h)}, \sigma_x^{(g,h)}, \sigma_y^{(g,h)}, \sigma_z^{(g,h)})$ with appropriate complex numbers A, and using Eqs. (6.46), one obtains for the correlation function:

$$\begin{aligned}
O^\dagger O = &\left(|A_0|^2 + \sum_i |A_i|^2 \right) \mathbb{1}_2^{(f)} \\
&+ \sum_i \left(\{A_0^* A_i + A_0 A_i^*\} + i \sum_{j,k} \epsilon_{ijk} A_j^* A_k \right) \sigma_i^{(f)}.
\end{aligned} \tag{6.47}$$

Since the $\sigma_{x,y,z}$ are summed over all sites and the order is alternating, the only contribution that is left is from the $\mathbb{1}_2$ term. What remains is

$$\begin{aligned}
G^{(g)}_{L_2} &= N\frac{\sin^2(\theta-\Theta)}{\omega-\omega_g+i\eta}\left[\frac{c'^2}{8}(|T_y-iP_y|^2+|T_x+iP_x|^2)+\frac{s'^2}{2}(|T_z|^2+|Q_2|^2)\right],\\
G^{(h)}_{L_2} &= \frac{N}{16}\frac{\sin^2 2(\theta-\Theta)}{\omega-\omega_h+i\eta}\left(|P_z|^2+\frac{1}{3}\left|\sqrt{3}P_{A_{1g}}+Q_3\right|^2\right),\\
G^{(g)}_{L_3} &= N\frac{\cos^2(\theta-\Theta)}{\omega-\omega_g+i\eta}\left[\frac{s'^2}{8}(|T_y-iP_y|^2+|T_x+iP_x|^2)+\frac{c'^2}{4}(|Q_2|^2+|T_z|^2)\right],\\
G^{(h)}_{L_3} &= \frac{N}{8}\frac{1}{\omega-\omega_h+i\eta}\left[\frac{1}{2}(\sin 2\theta+\sin 2(\theta-\Theta))^2\,|P_z|^2\right.\\
&\quad +|T_y+i\cos 2\theta\ P_y|^2+|T_x-i\cos 2\theta\ P_x|^2\\
&\quad \left.+\frac{1}{2}\left|\sqrt{3}\sin 2\theta\ Q_3-\sin 2(\theta-\Theta)\left(P_{A_{1g}}+\tfrac{1}{\sqrt{3}}Q_3\right)\right|^2\right].
\end{aligned}\tag{6.48}$$

In the cubic limit, this reduces to

$$\begin{aligned}
G^{(g)}_{L_2} &= G^{(h)}_{L_2}=0,\\
G^{(g)}_{L_3} &= \frac{N}{6}\frac{1}{\omega-\omega_g+i\eta}\left[\frac{1}{4}(|T_y-iP_y|^2+|T_x+iP_x|^2)+(|Q_2|^2+|T_z|^2)\right],\\
G^{(h)}_{L_3} &= N\frac{1}{\omega-\omega_h+i\eta}\left[\frac{1}{6}\left(\frac{1}{3}|P_z|^2+|Q_3|^2\right)+\frac{1}{8}\left|T_y+\frac{i}{3}P_y\right|^2+\frac{1}{8}\left|T_x-\frac{i}{3}P_x\right|^2\right].
\end{aligned}\tag{6.49}$$

In the limit of strong spin-orbit coupling, the g and h doublets have the same energy. Because quite some broadening is expected for these high energy excitations even in the Mott insulating state (as discussed in Sec. 6.2), the two peaks are probably not resolvable and merge into one big peak. In that case, it is more interesting to study the total spectral weight of the g and h excitations.

The total spectral weight is obtained by integrating the cross sections of the g and h excitations over energy loss, and adding them up. In the formula for the cross section, the imaginary part of the Green's function yields

$$-\frac{1}{\pi}\lim_{\eta\to 0}\mathfrak{Im}\{\frac{1}{\omega-\omega_g+i\eta}\}=-\frac{1}{\pi}\lim_{\eta\to 0}\frac{-\eta}{(\omega-\omega_g)^2+\eta^2}=\delta(\omega-\omega_g).\tag{6.50}$$

In the cubic limit with unrotated octahedra, one finds

$$I^{(g+h)}_{L_3}=\frac{N}{6}\left[\sum_{i\in\{x,y,z\}}\left(|T_i|^2+\frac{1}{3}|P_i|^2\right)+|Q_2|^2+|Q_3|^2\right].\tag{6.51}$$

The polarization factors nicely group together, yielding the O_h invariants

$$\sum_i |T_i|^2 = 1 - 2\sum_j \epsilon_j^* \epsilon_j \epsilon_j'^* \epsilon_j' + |\boldsymbol{\epsilon} \cdot \boldsymbol{\epsilon}'|^2 , \tag{6.52}$$

$$\sum_i |P_i|^2 = 1 - |\boldsymbol{\epsilon} \cdot \boldsymbol{\epsilon}'|^2 , \tag{6.53}$$

$$\sum_i |Q_i|^2 = 2\sum_j \epsilon_j^* \epsilon_j \epsilon_j'^* \epsilon_j' - \frac{2}{3} |\boldsymbol{\epsilon}'^* \cdot \boldsymbol{\epsilon}|^2 , \tag{6.54}$$

which add up to

$$I^{(g+h)}(\boldsymbol{\epsilon}', \boldsymbol{\epsilon}) = \frac{N}{9} \left[2 + |\boldsymbol{\epsilon}' \cdot \boldsymbol{\epsilon}|^2 - |\boldsymbol{\epsilon}'^* \cdot \boldsymbol{\epsilon}|^2 \right] . \tag{6.55}$$

In case of linear incoming or outgoing polarization, the intensity is independent of the polarization vectors. This entails that when the outgoing polarization is not measured, as is the case in all RIXS experiments done so far, the intensity is independent of the polarization vectors[2]. A non-trivial polarization dependence can only arise when both incoming and outgoing X-rays are circularly polarized.

6.3.4 Iridium L edge cross section – Special cases

We now specialize the cross sections obtained above to some geometries often used in experiments. We consider transferred momenta along the $\Gamma - M$ and $\Gamma - X$ directions [$\Gamma = (0,0)$, $X = (\pi, 0)$ and $M = (\pi, \pi)$], and take the scattering angle to be 90°. The incoming polarization is chosen to be linear, while the outgoing polarization is not detected. Along the $\Gamma - X$ path through the BZ, the polarization vectors are

$$\boldsymbol{\epsilon}_\pi = \begin{pmatrix} \cos\varphi \\ 0 \\ \sin\varphi \end{pmatrix} , \quad \boldsymbol{\epsilon}_\sigma = \begin{pmatrix} 0 \\ 1 \\ 0 \end{pmatrix} , \quad \boldsymbol{\epsilon}_\pi' = \begin{pmatrix} -\sin\varphi \\ 0 \\ \cos\varphi \end{pmatrix} , \quad \boldsymbol{\epsilon}_\sigma' = \boldsymbol{\epsilon}_\sigma . \tag{6.56}$$

π and σ mean, respectively, polarization parallel and perpendicular to the scattering plane. φ is the angle of the incoming X-rays with the normal to the IrO_2 planes. Along the $\Gamma - M$ path,

$$\boldsymbol{\epsilon}_\pi = \begin{pmatrix} \frac{1}{\sqrt{2}} \cos\varphi \\ \frac{1}{\sqrt{2}} \cos\varphi \\ \sin\varphi \end{pmatrix} , \quad \boldsymbol{\epsilon}_\sigma = \frac{1}{\sqrt{2}} \begin{pmatrix} -1 \\ 1 \\ 0 \end{pmatrix} , \quad \boldsymbol{\epsilon}_\pi' = \begin{pmatrix} -\frac{1}{\sqrt{2}} \sin\varphi \\ -\frac{1}{\sqrt{2}} \sin\varphi \\ \cos\varphi \end{pmatrix} , \quad \boldsymbol{\epsilon}_\sigma' = \boldsymbol{\epsilon}_\sigma . \tag{6.57}$$

The angle φ is related to $\mathbf{q}$. In 90° scattering geometry, the total transferred momentum (at an incident energy of 11.2 keV at the L_3 edge [223]) is ≈ 8.05 Å^{-1}

[2] This can be seen as follows: when the outgoing photon's polarization is not measured, it is summed over. One can choose to sum over two orthogonal linear polarization vectors, which makes $\boldsymbol{\epsilon}'^* = \boldsymbol{\epsilon}'$, and the polarization vectors cancel in Eq. (6.55).

while the X-point is at ≈ 0.808 Å^{-1} [223]. The X-rays carry an order of magnitude more momentum than needed to probe the BZ. It is therefore reasonable to approximate $\varphi \approx 45^\circ$ as constant: it varries 5.7° around 45° (assuming one stays in the first 2D Brillouin zone). This fact greatly diminishes the asymmetry effects between $+\mathbf{q}$ and $-\mathbf{q}$ that are so important in the cuprates (see Secs. 4.5.2 and 4.6.2).

Note that the integrated weight of the $J_{\text{eff}} = 3/2$ excitations are polarization-independent for linearly polarized light: $I^{(g+h)} = 2N/9$. For the $J_{\text{eff}} = 1/2$ excitations, we calculate 4 different cases: $\mathbf{q}$ towards X and M, and incoming π and σ polarization. Abbreviating $\cos\alpha = c_\alpha$ etc, the single- and two-magnon intensity in each case is

$$I^{(1)}_{X\pi} \propto \frac{N}{18}\left[\frac{s_\alpha^2}{2}(1+s_\varphi^2)(u_\mathbf{q}+v_\mathbf{q})^2 + \frac{c_\alpha^2}{2}(1+s_\varphi^2)(u_\mathbf{q}-v_\mathbf{q})^2 + c_\varphi^2(u_\mathbf{q}-v_\mathbf{q})^2\right] \times \delta(\omega-\omega_\mathbf{q}), \tag{6.58}$$

$$I^{(2)}_{X\pi} \propto \frac{1}{9}(1+s_\varphi^2)\sum_\mathbf{k}\left[s_\alpha^2\left(u_{\mathbf{k}+\mathbf{q}}v_\mathbf{k}+u_\mathbf{k}v_{\mathbf{k}+\mathbf{q}}\right)^2 + c_\alpha^2\left(u_{\mathbf{k}+\mathbf{q}}v_\mathbf{k}-u_\mathbf{k}v_{\mathbf{k}+\mathbf{q}}\right)^2\right] \times \delta(\omega-\omega_{\mathbf{k}+\mathbf{q}}-\omega_\mathbf{k}), \tag{6.59}$$

$$I^{(1)}_{X\sigma} \propto \frac{N}{18}\left[\frac{s_\alpha^2}{2}c_\varphi^2(u_\mathbf{q}+v_\mathbf{q})^2 + \frac{c_\alpha^2}{2}c_\varphi^2(u_\mathbf{q}-v_\mathbf{q})^2 + s_\varphi^2(u_\mathbf{q}-v_\mathbf{q})^2\right]\delta(\omega-\omega_\mathbf{q}), \tag{6.60}$$

$$I^{(2)}_{X\sigma} \propto \frac{1}{9}c_\varphi^2\sum_\mathbf{k}\left[s_\alpha^2\left(u_{\mathbf{k}+\mathbf{q}}v_\mathbf{k}+u_\mathbf{k}v_{\mathbf{k}+\mathbf{q}}\right)^2 + c_\alpha^2\left(u_{\mathbf{k}+\mathbf{q}}v_\mathbf{k}-u_\mathbf{k}v_{\mathbf{k}+\mathbf{q}}\right)^2\right] \times \delta(\omega-\omega_{\mathbf{k}+\mathbf{q}}-\omega_\mathbf{k}), \tag{6.61}$$

$$I^{(1)}_{M\pi} \propto \frac{N}{18}\left[s_\alpha^2 s_\varphi^2(u_\mathbf{q}+v_\mathbf{q})^2 + c_\varphi^2(u_\mathbf{q}-v_\mathbf{q})^2 + c_\alpha^2(u_\mathbf{q}-v_\mathbf{q})^2\right]\delta(\omega-\omega_\mathbf{q}), \tag{6.62}$$

$$I^{(2)}_{M\pi} \propto \frac{2}{9}\sum_\mathbf{k}\left[s_\alpha^2\left(u_{\mathbf{k}+\mathbf{q}}v_\mathbf{k}+u_\mathbf{k}v_{\mathbf{k}+\mathbf{q}}\right)^2 + c_\alpha^2 s_\varphi^2\left(u_{\mathbf{k}+\mathbf{q}}v_\mathbf{k}-u_\mathbf{k}v_{\mathbf{k}+\mathbf{q}}\right)^2\right] \times \delta(\omega-\omega_{\mathbf{k}+\mathbf{q}}-\omega_\mathbf{k}), \tag{6.63}$$

$$I^{(1)}_{M\sigma} \propto \frac{N}{18}\left[s_\alpha^2 c_\varphi^2(u_\mathbf{q}+v_\mathbf{q})^2 + s_\varphi^2(u_\mathbf{q}-v_\mathbf{q})^2\right]\delta(\omega-\omega_\mathbf{q}), \tag{6.64}$$

$$I^{(2)}_{M\sigma} \propto \frac{2}{9}c_\alpha^2 c_\varphi^2\sum_\mathbf{k}\left(u_{\mathbf{k}+\mathbf{q}}v_\mathbf{k}-u_\mathbf{k}v_{\mathbf{k}+\mathbf{q}}\right)^2\delta(\omega-\omega_{\mathbf{k}+\mathbf{q}}-\omega_\mathbf{k}). \tag{6.65}$$

The resulting spectra are displayed in Fig. 6.1, assuming $\varphi \approx 45^\circ$ and $\alpha = 8^\circ$. The (pseudo-)magnon results are very similar to the cuprates: the single-magnon intensity peaks strongly at the antiferromagnetic ordering vector (π, π). Also, the two-magnon intensity at $(0, 0)$ is suppressed while the two-magnon DOS is highest there [see Fig. 4.5(b)]. The doublet to quartet excitations have an energy of $(3/2)\lambda$. Although λ is measured to be around 380 meV, the exact ratio of λ

to J is not known. The rough theoretical estimate $J \approx 45$ meV [214] would put $(3/2)\lambda/J$ at 12.7, but that could well be off by 50% or more. High resolution RIXS experiments would be a much better way to precisely determine this ratio. We therefore regard the ratio as a free parameter in our theory, and put it at 8 for the moment. In Fig. 6.2, spectra at several transferred momenta are shown. These figures are vertical cuts through Fig. 6.1. The spectral weight of the different types of excitations is compared in Fig. 6.3.

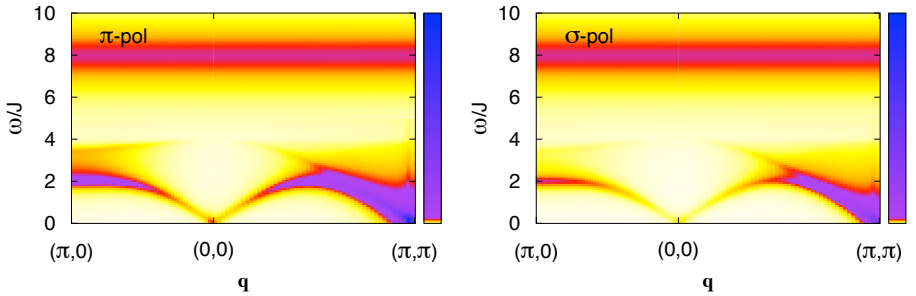

Figure 6.1: RIXS spectra of Sr_2IrO_4 at the Ir L_3 t_{2g} edge, including single- and two-magnon $J_{\text{eff}} = 1/2$ excitations and $J_{\text{eff}} = 3/2$ excitations. The latter are put at an energy of $8J$ with a phenomenological broadening of J (half-width at half-max). We have assumed that the system is dominated by 5d spin-orbit coupling, $\varphi = 45°$ and $\alpha = 8°$. The left panel shows the spectrum for incoming π polarization, and the right one for incoming σ polarization.

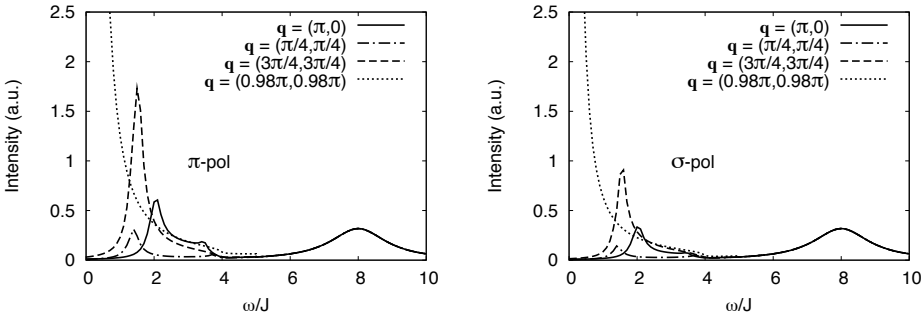

Figure 6.2: RIXS spectra of Sr_2IrO_4 at the Ir L_3 t_{2g} edge, including single- and two-magnon $J_{\text{eff}} = 1/2$ excitations and $J_{\text{eff}} = 3/2$ excitations. These spectra are vertical cuts through Fig. 6.1. The left panel shows several spectra for incoming π polarization, and the right one for incoming σ polarization.

A very striking feature of dominating spin-orbit coupling is the absence of

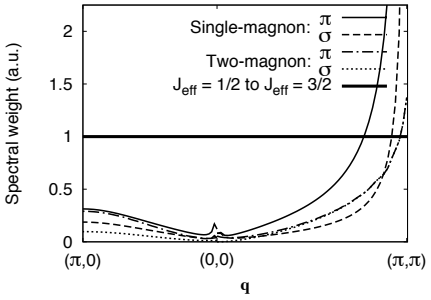

Figure 6.3: RIXS spectral weight of Sr_2IrO_4 at the Ir L_3 t_{2g} edge, obtained by integrating the different features of the spectra of Fig. 6.1 over energy loss. The units on the vertical axis are chosen such that the $J_{\text{eff}} = 1/2$ to $J_{\text{eff}} = 3/2$ excitations have spectral weight 1.

excitations in L_2 edge spectra. Looking at the L_3 edge with low energy resolution ($\sim$ 0.6 eV), it is impossible to see any details of the L_3 excitation spectra of Figs. 6.1 and 6.2 except for the total spectral weight. As is clear from Fig. 6.3, the total spectral weight strongly peaks at $\mathbf{q} = (\pi, \pi)$ and is lowest (but non-zero) at $\mathbf{q} = (0, 0)$. With a better energy resolution, one might be able to see the dispersion of the magnon excitations: at $\mathbf{q} = (\pi, \pi)$, the intense single-magnon peak disperses down to zero energy loss, from about $2J \approx 90$ meV at $\mathbf{q} = (\pi, 0)$ and $(\pi/2, \pi/2)$. RIXS can determine the values of λ and J up to the energy resolution of the experiment.

The results obtained in this chapter can easily be applied to other Ir compounds with octahedral crystal fields, such as the hexagonal Kitaev-Heisenberg model compounds A_2IrO_3 (A = Li, Na) [214, 215]. The collective response will be different, but the local scattering operators derived in Sec. 6.3.2 still apply.